The Egyptian Journal of Radiology and Nuclear Medicine (2015) **46**, 491–497

Egyptian Society of Radiology and Nuclear Medicine

**The Egyptian Journal of Radiology and Nuclear Medicine**

www.elsevier.com/locate/ejrnm
www.sciencedirect.com

ORIGINAL ARTICLE

# Reconstruction of head-to-knee voxel model for Syrian adult male of average height and weight

**Bashira Taleb** [a,*], **Ahmad Khadour** [a], **Abdalkader Bitar** [b]

[a] *Biomedical Engineering Department, College of Electrical and Mechanical Engineering, Damascus University, Syria*
[b] *Protection and Safety Department, Atomic Energy Commission, Damascus, Syria*

Received 25 September 2014; accepted 21 February 2015
Available online 13 March 2015

**KEYWORDS**

Digital voxel model;
Segmentation;
Specific Absorbed Fractions (SAF);
Monte Carlo method

**Abstract** *Purpose:* This study embodies the reconstruction of head to knee voxel model, named "SyrMan", of an adult living Syrian male of average height and weight. This model contains main organs of one adult man representing the average of a group of adult males (25–50) years. SyrMan model was reconstructed to be used for Monte Carlo simulations to calculate dosimetric quantities for radiation protection and medical purposes.
*Method:* The model was reconstructed from segmented CT images of a living volunteer who was 33 year-old, 172 cm in height, and 75 kg in weight. Masses of segmented organs were calculated and compared with previously published models.
*Results:* Specific Absorbed Fractions (SAFs) were calculated and tabulated for each considered source organ. Comparison of SAF values was carried out with Zubal model where some significant differences were found due to differences in organ masses and in anatomy between both models.
*Conclusion:* Comparisons with SAFs data of Zubal model accentuated the fact that the organ masses and the specific anatomy have a significant effect on SAFs. SyrMan model can be considered as the first model built in the Middle East region, and it is an important step toward the Syrian Reference Man.


## 1. Introduction

Early models representing the human body for radiation dosimetry were known in North America and Europe in the 1960s of the last century (1,2). Afterward, models for other racial ethnicities, such as Japanese, Chinese, and Korean models had been reconstructed (3–7). These models were reconstructed to be used in ionizing and/or non-ionizing radiation fields (7).

First models for human body were mostly homogeneous simple geometric forms such as spheres, cylinders or slabs and it based on surfaces that described by quadric equations and commonly referred to as "stylized" phantoms (1,2) (Fig. 1).

The first heterogeneous anthropomorphic model was created for the Medical Internal Radiation Dose (MIRD) by

* Corresponding author. Tel.: +963 966165842.
E-mail addresses: btalebtaleb@hotmail.com, btalebtalebtaleb@gmail.com (B. Taleb), abdbitar@gmail.com (A. Bitar).
Peer review under responsibility of Egyptian Society of Radiology and Nuclear Medicine.

http://dx.doi.org/10.1016/j.ejrnm.2015.02.010

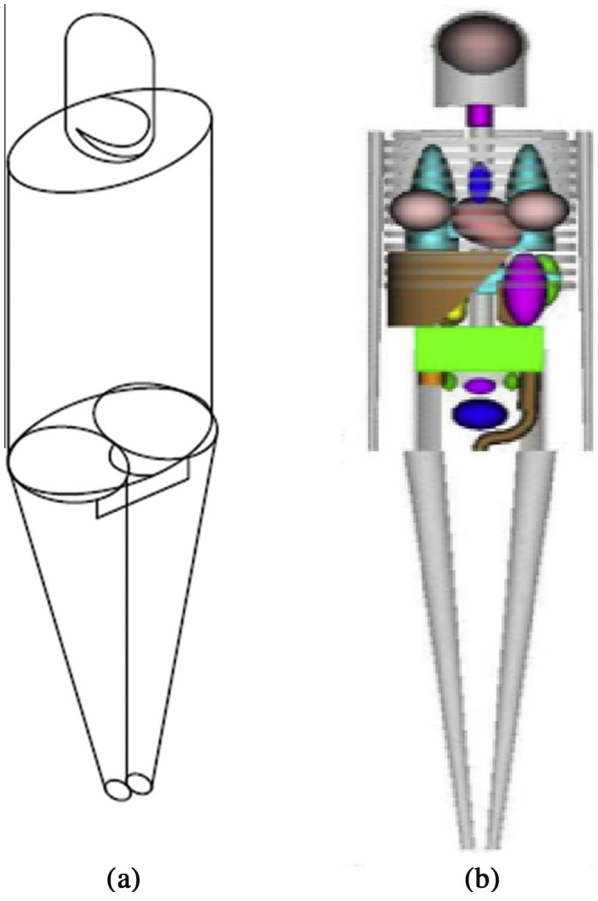


**Fig. 1** Stylized phantoms: (a) external vision of the adult male. (b) Skeleton and internal organs (7).

Snyder et al. (1969–1978) using constructive solid geometry (CSG) modeling techniques (1,2,4,8). This model, known as MIRD Phantom, was based on the concept of the "Reference Man" for radiation protection purposes (ICRP 1975). Reference Man was originally defined as being a 20–30 year-old Caucasian, weighing 70 kg and 170 cm in height (9).

After that, several models were developed, but they were not be able to describe accurately the realistic anatomy of the human body. It is clear, however, that the human anatomy is too complex to be realistically modeled with a limited set of simple equations (7).

With the emerging of computed tomography (CT) and magnetic resonance (MR) imaging techniques, researchers could visualize the internal structures of the body in three dimensions and store images in digital formats. This leads to the idea of creating voxel or tomographic phantoms depending on the real anatomy of the human body (4,7,8).

A tomographic image data set is composed of many slices (images); each image consists of two-dimensional (2D) pixel map representing a real anatomy.

Unlike stylized phantoms which are based on quadric surface equations, a voxel phantom contains a huge number of cubes gathered to denote various real anatomical structures (Fig. 2).

The reconstruction of a voxel phantom includes four common steps as follows: (1) obtain a set of tomographic images that cover the complete volume or most part of the body; (2) classify organs or tissues of interest from the original image slice; (3) identify the density and chemical composition of organs or tissues; and (4) index the segmented image slices into a 3D volume that can be used for 3D visualization and for Monte Carlo calculations.

First effort to reconstruct a voxel model was introduced by Gibbs et al., it was built from CT scans of a female cadaver and projected to calculate the effective dose from dental radiography (10,11); soon after, Williams et al. began to build a family of voxel models of various ages (12).

Zankl et al. started developing a family of 12 various voxel phantoms using CT images for healthy volunteers at GSF National Research Center for Environment and Health in Germany (12–15). Fig. 2a displays one of GSF family models named Golem voxel model.

Kramer et al., from Brazil, developed an adult male model named MAX06 and an adult female model named FAX06; both models were adjusted according to ICRP 89 reference body heights and organ masses (16,17).

Stabin and Yoriaz published SAF values based on Zubal et al. head-torso model named "Voxel Man" which was reconstructed of CT images with dimensions similar to the MIRD 5 stylized phantom with Improvements to with MRI scan data (18,19).

VIP-Man phantom was the first model that based on a cross-sectional color photographic images of a cadaver (Fig. 2b). A data set was collected depending on color photographic anatomical slice images of the 39 year-old male acquired by the Visible Human Project (VHP) of the American National Library of Medicine (20,21).

Jones created NORMAN phantom which was based on whole body MRI scan data of a healthy volunteer. The exact dimensions of the voxels were scaled so that height and mass of the segmented model agreed with the values of Reference Man (8).

Most of the tomographic phantoms described above were based on Caucasian medical images. Subsequently, several works were accomplished using primary data from different racial ethnicities (3–7).

The first Asian adult male phantom Otoko was developed by Saito et al. from whole body CT data of a patient whose external dimensions are in agreement with the Japanese Reference Man (5,6). Also several Korean phantoms have been developed by researchers Lee and Kim (3,4).

The voxel computational phantoms were combined with various Monte Carlo codes that simulated the radiation transport in human material (7,8,11,12,18–20).

Due to the lack of detailed voxel model for the Middle East region, this study represents the reconstruction of head to knee voxel model, named "SyrMan", of an adult living Syrian male of average height and weight (Fig. 2c). SyrMan was then exploited in internal dosimetry calculations using Monte Carlo simulations.

## 2. Methods

### *2.1. CT data*

The primary data were obtained in DICOM format from computed tomographic examination of a single volunteer.

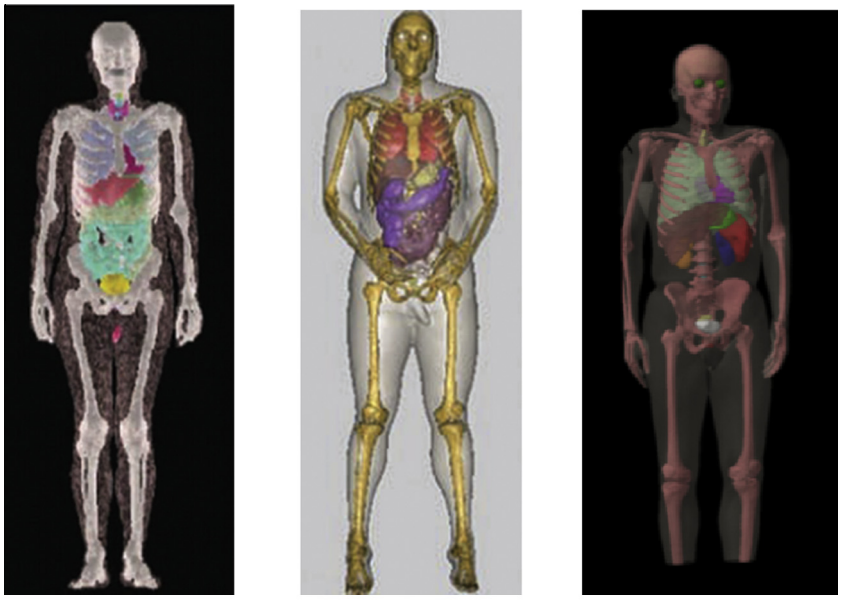


**Fig. 2** (a) GSF Golem voxel phantom, (b) VIP-Man voxel phantom and (c) SyrMan voxel phantom.

This volunteer represents the average, in weight and height, of a group of 262 males aged between 25 and 50 years. The volunteer was 33 year-old male, 172 cm in height, and 75 kg in weight. The slices covered the body from head to mid-legs. The volunteer was lying supine with arms parallel and alongside the body. The examination was performed with Siemens scanner Somatom Sensation 64 at 120 kVp. The number of slices was 500 with 3 mm of thickness for each slice which consisted of a matrix of $512 \times 512$ pixels. The plan resolution is 1.024 pixel in each millimeter, therefore, the voxel size is $0.98 \times 0.98$ mm$^2$. The primary images had 16 bits per pixel, 12 bits stored, 11 bit height, size storage for each image is 515k, and the display range is 450–1050.

### 2.2. Segmentation tools and method

#### 2.2.1. Medical image segmentation techniques

Medical image segmentation techniques play an important role in human body modeling. Many algorithms were developed to provide noninvasive information of internal anatomical structures in human body. These algorithms vary widely depending on the specific application. Generally, no segmentation technique works for all the applications (22). The most popular medical image segmentation techniques can be divided into five main categories: Rule-based segmentation, Statistical inference segmentation, Atlas-based segmentation, Edge-based segmentation and Deformable models based segmentation (23,24). In this study, different segmentation methods were used in order to reconstruct the "SyrMan" model.

#### 2.2.2. "SyrMan" model Segmentation method

After obtaining the tomographic images in DICOM format, the first step was doing smart segmentation using Eclipse software. Eclipse program is a TPS (Treatment Planning System) software for external radiotherapy by linear accelerator. In result, 17 tissues and organs were segmented. The segmented organs and tissues were brain, pituitary gland, eyes, thyroid gland, heart, lungs, spleen, pancreas, liver, trachea, pancreas, kidneys, bladder, stomach, prostate, rectum, bones (thigh bone, brachium bone, fragment bone, rachis bone, pelvis bone, cervical spinal cord, collarbone, sternum bone, thorax, marrow and skull).

Smart segmentation was used to segment lungs and bones, while the rest of organs were segmented manually with the help of radiologist and using human's anatomy atlases (25,26). The segmented images were obtained by doing screen capture for each slice after finishing smart and manual segmentations. As a result, each organ and tissue had its own color in the segmented images. The dimensions of the captured images were $1018 \times 1591$ pixels, and the voxel size was $0.4 \times 0.4 \times 3$ mm$^3$. In order to adapt the images for Monte Carlo simulations, automatic image processing was also carried out by Matlab program to get the final segmented images after manual processing by Photoshop7. The segmented images were reconstructed to get 3D model with the help of the Eclipse software (Fig. 2c).

### 2.3. Deposited energy

MCNP4C2 code (Mont Carlo N-Particle) published by Briesmeister (27) was used to obtain the deposited energy in different organs and tissues. Specific Absorbed Fractions (SAFs) for photons were then calculated for many combinations (target, source). Source organ emits isotropically monoenergetic photons which are supposed to be homogeneously distributed in the whole volume of the considered source organ. These SAF values can be used to calculate the dose-equivalent rate in a given target organ from a given radionuclide that is present in a given source organ.

Absorbed dose rate to target tissue from nuclear transformations in a source tissue is defined as:

$$\overline{\dot{D}} = \frac{\mathrm{NEA}\varnothing}{m} \tag{1}$$

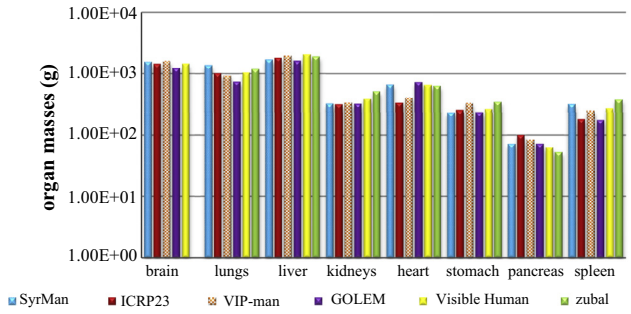


**Fig. 3** Comparison between organ masses of some voxel models versus SyrMan model.

∅: absorbed fraction of the energy emitted by radioactivity in the source region that is absorbed in the target region (28). Δ = NE: mean energy emitted per nuclear transition. $m$: mass of the target. $A$: radioactivity transformations.

SAF is defined as the absorbed fraction per unit mass of the target:

$$\Phi = \frac{\varnothing}{m} \tag{2}$$

Also, cumulated activity represents the total number of radioactive transformations in the source region over time of interest:

$$\widetilde{A} = \int_{t1}^{t2} A(t)dt \tag{3}$$

The mean absorbed dose to the target volume from nuclear transitions in the source region results from integration of the absorbed dose rate over time interval:

$$\overline{D} = \widetilde{A}\Delta\Phi = \widetilde{A}S \tag{4}$$

Photon SAFs were calculated for main organs of "SyrMan" model and were compared with those for previous published model (18).

### 2.4. Monte Carlo simulations

Each simulation run fifty million histories for each considered photon energy.

Results were obtained in approximately 231 h for all organs, for 12 initial photon energies of 0.01, 0.015, 0.02, 0.03, 0.05, 0.1, 0.2, 0.3, 0.5, 1, 1.5, 2 and 4 MeV. The tally

**Table 1** Relative differences (in %) between "SyrMan" and five models for height, weight, and some organs' masses.

| | Zubal | Visible human | GOLEM | ICRP 23 | VIP-man |
|---|---|---|---|---|---|
| Height | −1.16 | 4.65 | 2.32 | −1.16 | 7.7 |
| Weight | −0.92 | 36.06 | −8.98 | −8.17 | 15.8 |
| Brain | – | −7.79 | −26.46 | −7.79 | 2.13 |
| Thyroid | – | 48.48 | 36.49 | 18.08 | 40.64 |
| Lungs | −13.87 | −31.14 | −84.57 | −34.55 | −47.78 |
| Heart | −4.37 | −2 | 9.24 | −96.9 | −62.97 |
| Liver | 14.3 | 18 | −4.911 | 7.211 | 13.81 |
| Stomach | 32.7 | 10.94 | 1.38 | 8.09 | 29.19 |
| Spleen | 15.68 | −17.46 | −79.58 | −73.59 | −28.06 |
| Pancreas | −36.05 | −14.71 | 0.28 | 28.3 | 13.51 |
| Kidneys | 37.34 | 17.06 | −0.52 | −2.47 | 5.28 |

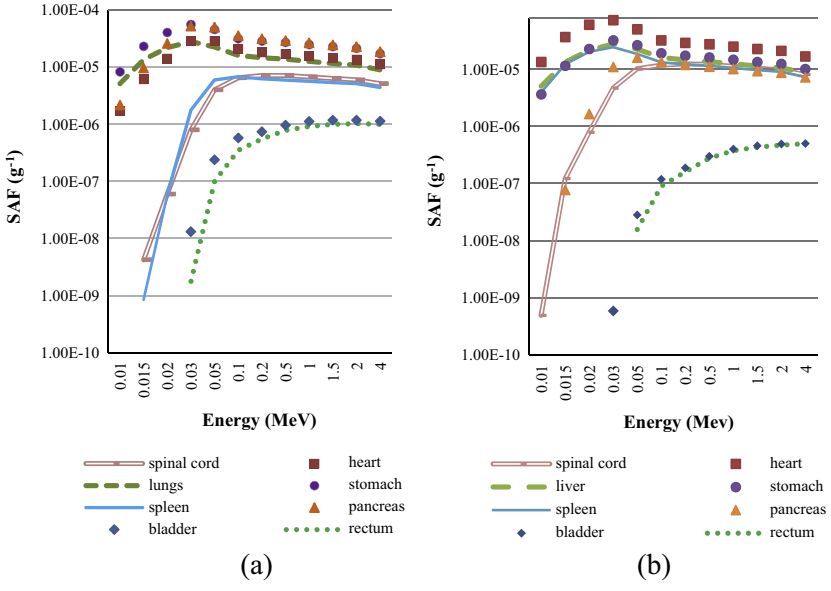


**Fig. 4** SAF values, for different targets, versus initial photon energy for SyrMan model; (a) source organ is liver and (b) source organ is lungs.

**Table 2** Specific absorbed fractions ($g^{-1}$) as a function of initial photon energy (MeV) – source organ is LIVER.

| Target | Energy (MeV) | | | | | | | | | | | |
|---|---|---|---|---|---|---|---|---|---|---|---|---|
| | 0.01 | 0.015 | 0.02 | 0.03 | 0.05 | 0.1 | 0.2 | 0.5 | 1 | 1.5 | 2 | 4 |
| Bladder | 0.00E+00 | 0.00E+00 | 0.00E+00 | 1.32E−08 | 2.39E−07 | 5.74E−07 | 7.38E−07 | 9.63E−07 | 1.12E−06 | 1.17E−06 | 1.18E−06 | 1.13E−06 |
| Heart | 1.72E−06 | 6.09E−06 | 1.41E−05 | 2.83E−05 | 2.86E−05 | 2.06E−05 | 1.81E−05 | 1.70E−05 | 1.56E−05 | 1.45E−05 | 1.35E−05 | 1.12E−05 |
| Liver | 5.79E−04 | 5.43E−04 | 4.83E−04 | 3.39E−04 | 1.76E−04 | 1.04E−04 | 9.90E−05 | 9.78E−05 | 8.88E−05 | 8.00E−05 | 7.27E−05 | 5.44E−05 |
| Lungs | 5.12E−06 | 1.35E−05 | 2.19E−05 | 2.79E−05 | 2.24E−05 | 1.60E−05 | 1.46E−05 | 1.38E−05 | 1.26E−05 | 1.16E−05 | 1.08E−05 | 8.90E−06 |
| Pancreas | 2.16E−06 | 9.61E−06 | 2.58E−05 | 5.18E−05 | 4.97E−05 | 3.52E−05 | 3.12E−05 | 2.91E−05 | 2.65E−05 | 2.43E−05 | 2.263E−05 | 1.851E−05 |
| Prostate | 0.00E+00 | 0.00E+00 | 0.00E+00 | 4.43E−09 | 1.02E−07 | 3.28E−07 | 4.82E−07 | 6.86E−07 | 8.36E−07 | 9.16E−07 | 9.32E−07 | 9.38E−07 |
| Rectum | 0.00E+00 | 0.00E+00 | 0.00E+00 | 1.78E−09 | 1.00E−07 | 3.50E−07 | 5.52E−07 | 7.79E−07 | 9.14E−07 | 9.98E−07 | 1.02E−06 | 9.97E−07 |
| Spinal cord | 0.00E+00 | 4.23E−09 | 5.95E−08 | 7.89E−07 | 3.98E−06 | 6.48E−06 | 7.11E−06 | 7.10E−06 | 6.70E−06 | 6.32E−06 | 5.96E−06 | 5.10E−06 |
| Spleen | 0.00E+00 | 0.00E+00 | 5.74E−08 | 1.77E−06 | 5.93E−06 | 6.74E−06 | 6.21E−06 | 5.92E−06 | 5.64E−06 | 5.34E−06 | 5.10E−06 | 4.38E−06 |
| Stomach | 8.29E−06 | 2.31E−05 | 4.03E−05 | 5.55E−05 | 4.54E−05 | 3.14E−05 | 2.85E−05 | 2.71E−05 | 2.47E−05 | 2.28E−05 | 2.12E−05 | 1.72E−05 |
| Trachea | 0.00E+00 | 6.10E−09 | 2.18E−07 | 2.25E−06 | 4.93E−06 | 4.72E−06 | 4.32E−06 | 4.01E−06 | 3.76E−06 | 3.46E−06 | 3.324E−06 | 2.807E−06 |

**Table 3** Specific absorbed fractions ($g^{-1}$) as a function of initial photon energy (MeV) - Source organ is Lungs.

| Target | Energy (MeV) | | | | | | | | | | | |
|---|---|---|---|---|---|---|---|---|---|---|---|---|
| | 0.01 | 0.015 | 0.02 | 0.03 | 0.05 | 0.1 | 0.2 | 0.5 | 1 | 1.5 | 2 | 4 |
| Bladder | 0.00E+00 | 0.00E+00 | 0.00E+00 | 5.85E−10 | 2.82E−08 | 1.19E−07 | 1.89E−07 | 3.01E−07 | 4.02E−07 | 4.61E−07 | 4.93E−07 | 5.06E−07 |
| Heart | 1.34E−05 | 3.68E−05 | 6.07E−05 | 7.28E−05 | 5.03E−05 | 3.22E−05 | 2.91E−05 | 2.76E−05 | 2.50E−05 | 2.28E−05 | 2.11E−05 | 1.68E−05 |
| Liver | 5.07E−06 | 1.34E−05 | 2.17E−05 | 2.79E−05 | 2.26E−05 | 1.61E−05 | 1.46E−05 | 1.38E−05 | 1.25E−05 | 1.15E−05 | 1.07E−05 | 8.63E−06 |
| Lungs | 6.62E−04 | 5.22E−04 | 3.63E−04 | 1.71E−04 | 6.94E−05 | 4.24E−05 | 4.20E−05 | 4.13E−05 | 3.62E−05 | 3.15E−05 | 2.77E−05 | 1.84E−05 |
| Pancreas | 0.00E+00 | 7.73E−08 | 1.65E−06 | 1.10E−05 | 1.60E−05 | 1.34E−05 | 1.20E−05 | 1.12E−05 | 1.02E−05 | 9.33E−06 | 8.71E−06 | 7.26E−06 |
| Prostate | 0.00E+00 | 0.00E+00 | 0.00E+00 | 3.47E−22 | 1.34E−08 | 6.70E−08 | 1.26E−07 | 2.25E−07 | 3.19E−07 | 3.74E−07 | 4.00E−07 | 4.34E−07 |
| Rectum | 0.00E+00 | 0.00E+00 | 0.00E+00 | 0.00E+00 | 1.57E−08 | 9.03E−08 | 1.61E−07 | 2.78E−07 | 3.76E−07 | 4.34E−07 | 4.70E−07 | 5.00E−07 |
| Spinal cord | 4.89E−10 | 1.22E−07 | 7.91E−07 | 4.70E−06 | 1.02E−05 | 1.19E−05 | 1.24E−05 | 1.23E−05 | 1.13E−05 | 1.04E−05 | 9.77E−06 | 8.10E−06 |
| Spleen | 3.93E−06 | 1.23E−05 | 2.03E−05 | 2.44E−05 | 1.86E−05 | 1.33E−05 | 1.21E−05 | 1.15E−05 | 1.06E−05 | 9.68E−06 | 9.03E−06 | 7.30E−06 |
| Stomach | 3.67E−06 | 1.16E−05 | 2.29E−05 | 3.24E−05 | 2.66E−05 | 1.91E−05 | 1.74E−05 | 1.62E−05 | 1.47E−05 | 1.35E−05 | 1.25E−05 | 1.01E−05 |
| Trachea | 2.27E−05 | 5.18E−05 | 7.62E−05 | 7.62E−05 | 4.60E−05 | 2.92E−05 | 2.71E−05 | 2.56E−05 | 2.32E−05 | 2.11E−05 | 1.94E−05 | 1.521E−05 |

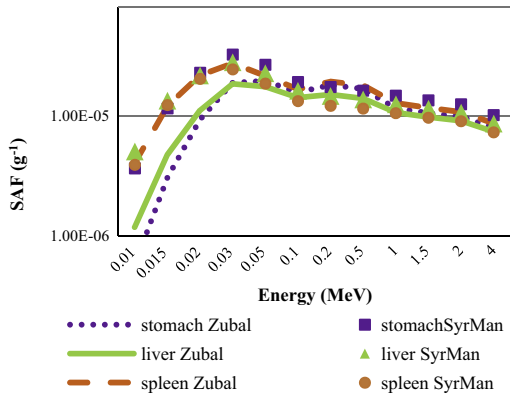


**Fig. 5** Comparison of SAF values between SyrMan and Zubal where source organ is lungs and target organs are liver, spleen and stomach.

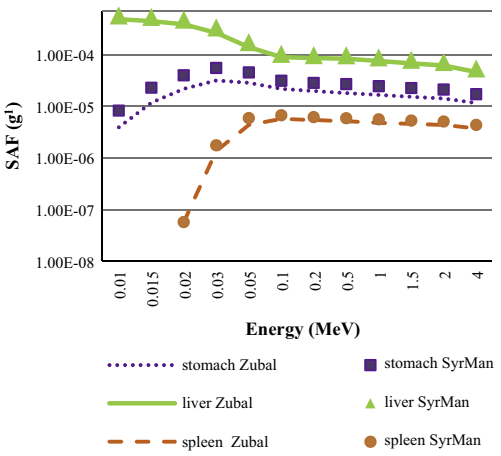


**Fig. 6** Comparison of SAF values between SyrMan and Zubal where source organ is liver and target organs are spleen, liver, and stomach.

*F8 was used to obtain the energy deposited, from both photons and secondary electrons, in MeV per source particle.

Energy deposited in all voxels of a target organ was summed, and this value was divided by the initial energy emitted in the source to obtain the absorbed fraction (AF); subsequently, the SAF was calculated as the AF divided by the known mass of the target organ.

## 3. Results

### 3.1. Organs masses

The volume of each tissue equals the volume of one voxel times the number of voxels constitutes that tissue. The masses of tissues were calculated by multiplying the volume of each tissue with the appropriate tissue density.

For "SyrMan" model, the following five different elemental tissue compositions and resulting mass densities were considered: spleen, brain, pancreas, bladder and prostate as ($\rho$ = 1.040 g cm$^{-3}$), lung as ($\rho$ = 0.260 g cm$^{-3}$), eye lens as ($\rho$ = 1.070 g cm$^{-3}$), thyroid, heart, stomach and kidneys as ($\rho$ = 1.050 g cm$^{-3}$), liver as ($\rho$ = 1.060 g cm$^{-3}$) (7,9,15,18,20). Fig. 3 shows a comparison of organ masses between "SyrMan" model versus those for ICRP23, VIPman, GOLEM, and Visible Human models. Relative differences internal organ masses, height, and weight between "SyrMan" model and the five mentioned models, were also calculated (Table 1).

### 3.2. Specific absorbed fractions for photons

SAFs for photons for various source and target organ combinations were calculated. Fig. 4 illustrates SAF values calculated for SyrMan model where the source organ is liver (Fig. 4a) and lungs (Fig. 4b).

SAF values were tabulated for each simulated source organ in function of initial photon energy (Tables 2 and 3).

Comparisons were carried out with the SAFs published by Stabin and Yoriyaz (18) for Zubal phantom. Figs. 5 and 6 show SAF comparisons between SyrMan and Zubal where source organ is lungs and liver respectively.

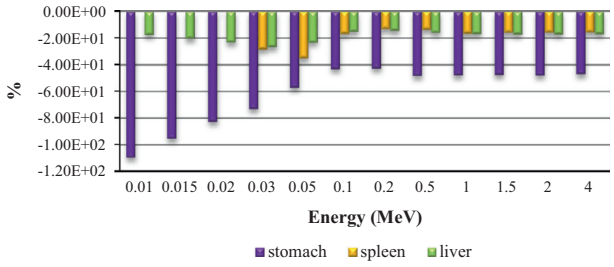


**Fig. 7** Relative differences between SyrMan and Zubal for SAFs in spleen, stomach, and liver, from liver, for 12 photon energies.

Fig. 7 shows relative differences between SAF values of both models where the source organ is liver.

## 4. Discussion

While some characteristics of SyrMan model, such as weight and height, were close to those of Zubal phantom, separate organ masses are considerably different in many cases. However, the comparison with SAF values of Zubal reveals that the curves have similar shapes but with some differences which can generally be related to differences in organ masses and to different anatomic structures between the comparative phantoms.

For example, liver mass differs about 14.3% between SyrMan and Zubal, therefore, SAFs(liver ← liver) for SyrMan were higher. Also, spleen mass differs about 15.75% between SyrMan and Zubal, so SAFs(spleen ← liver) for SyrMan were considerably higher, similarly SAFs(stomach ← liver) for SyrMan were higher whereas stomach mass differs about 32.7% between SyrMan and Zubal.

## 5. Conclusion

Most of anthropomorphic phantoms were representing special racial ethnicities such as the Chinese, Japanese, Korean, as well as Caucasian reference model. SyrMan head-to-knee 3D

voxel model was reconstructed to represent, as much as possible, middle-east anatomic structures. SyrMan embodies the average of adult males aged from 25 to 50 years. This model was used in internal dose calculations and can be also employed for radiation protection purposes. Specific Absorbed Fractions (SAFs) were calculated, and tabulated, for many source-target combinations using Monte Carlo simulations. Comparisons with previous SAFs data emphasized the fact that the organ masses and the individual anatomy have an important effect on SAFs.

## Conflict of interest

None declared.

## References


(1) Snyder WS, Fisher Jr HL. Distribution of dose in the body from a source of gamma rays distributed uniformly in an organ. Report No. ORNL-4168. USA (TN): Oak Ridge National Laboratory; 1967.

(2) Snyder WS, Fisher Jr HL, Ford MR, Warner GG. Estimates of specific absorbed fractions for photon sources uniformly distributed in various organs of a heterogeneous phantom. J Nucl Med 1969;3:52–7.

(3) Lee C, Lee C, Park SH, Lee JK. Development of the two Korean adult tomographic computational phantoms for organ dosimetry. Med Phys 2006;33(2):380–90.

(4) Lee C, Lee JK. Computational anthropomorphic phantoms for radiation protection dosimetry: evolution and prospects. Nucl Eng Technol 2006;38(3):239–50.

(5) Saito K, Wittmann A, Koga S, Ida Y, Kamei T, Funabiki J, et al. Construction of a computed tomographic phantom for a Japanese male adult and dose calculation system. Radait Environ Biophys 2001;40(1):69–75.

(6) Tanaka G, Nakahara Y, Nakazima Y. Japanese reference man 1988-IV. Studies on the weight and size of internal organs of Normal Japanese. Nihon Igaku Hoshasen Gakkai Zasshi 1989;49(3):344–64.

(7) Xu XG, Eckerman KF. Handbook of anatomical models for radiation dosimetry. Boca Raton (FL): CRC Press/Taylor and Francis Group; 2009.

(8) Jones DG. A realistic anthropomorphic phantom for calculating organ doses arising from external photon irradiation. Radiat Prot Dosimetry 1997;72:21–9.

(9) International Commission on Radiological Protection (ICRP). Report of the Task Group on Reference Man. ICRP Publication 23. New York: Pergamon; 1975.

(10) Gibbs SJ, Pujol A, Chen TS, Malcolm AW. Computer-simulation of patient dose from dental radiography. J Dent Res 1984; 63(209).

(11) Gibbs SJ, Pujol A, Chen TS, Malcolm AW, James AE. Monte-Carlo computation of patient risk from dental radiography. Invest Radiol 1985;20(S23).

(12) Williams G, Zankl M, Abmayr W, Veit R, Drexler G. The calculation of dose from external photon exposures using reference and realistic human phantoms and Monte-Carlo methods. Phys Med Biol 1986;31(449).

(13) Zankl M, Petoussi-Henss N, Fill U, Regulla D. The GSF family of voxel phantoms. Phys Med Biol 2002;47:106–89.

(14) Zankl M, The GSF. Voxel computational phantom family. Boca Raton (FL): CRC Press/Taylor and Francis Group; 2009.

(15) Zankl M, Wittmann A. The adult male voxel model "Golem" segmented from whole-body CT patient data. Radiat Environ Biophys 2001;40:153–62.

(16) Kramer R, Khoury HJ, Vieira JW, Kawrakow I. Skeletal dosimetry in the MAX06 and the FAX06 phantoms for external exposure to photons based on vertebral 3D-micro CT images. Phys Med Biol 2006:51–6265.

(17) Kramer R, Khoury HJ, Vieira JW, Loureiro ECM, LimaV JM, Lima FRA, et al. All about FAX: a female adult voxel phantom for Monte Carlo calculation in radiation protection dosimetry. Phys Med Biol 2004;49(23):5203–16.

(18) Stabin MG, Yoriyaz H. Photon specific absorbed fractions calculated in the trunk of an adult malevoxel-based phantom. Health Phys 2002;82(1):21–44.

(19) Zubal IG, Harrell CR, Smith EO, Rattner Z, Gindi G, Hoffer PB. Computerized 3 dimensional segmented human anatomy. Med Phys 1994;21:299–302.

(20) Xu XG, Chao TC, Bozkurt A. VIP-man: an image-based whole-body adult male model constructed from color photographs of the visible human project for multi-particle Monte Carlo calculations. Health Phys 2000;78:476–86.

(21) Xu XG, Chao TC, Bozkurt A, Shi Ch, Zhang J. The 3D and 4D VIP-man computational phantoms. Boca Raton (FL): CRC Press/Taylor and Francis Group; 2009.

(22) Gonzalez RC, Woods RE. Digital image processing. 3rd ed. Upper Saddle River (NJ): Pearson Prentice Hall; 2008.

(23) Elnakib A, Gimel'farb G, Suri J, El-Baz A. Medical image segmentation: a brief survey. In: El-Baz A, Acharya R, Laine A, Suri J, editors. Handbook of multi modality state-of-the-art medical image segmentation and registration methodologies, vol. 2. New York: Springer-Verlag; 2011. p. 1–39.

(24) Alansary A, Soliman A, Khalifa F, Elnakib A, Mostapha M, Nitzken M, et al. MAP-based framework for segmentation of MR brain images based on visual appearance and prior shape. MIDAS J 2013;1:1–13.

(25) Kahle W. Color atlas and textbook of human anatomy, vol. 3. New York: Thieme Stuttgart; 2003.

(26) Moeller T, Reif E. Pocket atlas of sectional anatomy computed tomography and magnetic resonance imaging, vol. 2. New York: Thieme Stuttgart; 2001.

(27) Briesmeister JF. MCNPTM– a general Monte Carlo N-particle transport code version 4C. LANL/Los Alamos. LA-13709-M 2000.

(28) Howell RW, Wessels BW, Loevinger R. The MIRD perspective 1999. J Nucl Med 1999;40(1) [10S-3S].